Kinematic structural forward modeling for fault trajectory prediction in seismic interpretation

Mohammed, Alarfaj
Don, C., Lawton
CREWES, University of Calgary

Summary

The unique relationship between fault shape and hanging-wall deformation in extensional settings is explained by the rollover concepts. These concepts are modeled and described along with factors controlling deformational geometries such as fault shape, sedimentation and slip ratios, hanging-wall shear direction and shear angles. The concepts are applied to model and predict a fault deep shape from seismic images where the fault may not be visible.

Introduction

Rocks, when undergoing deformation, flow, bend or, in the case of faults, slip. Mapping faults is crucial in hydrocarbon exploration and production as faults can act as a sealing mechanism for a potential trap, or a conduit for fluids in tight formations. Faults are inferred in the subsurface by seismic imaging which is an indirect representation of the subsurface measured in two-way time. Seismic imaging is often associated with signal distortion and limitations in temporal and spatial resolution. Seismic data may be subject to misinterpretation since it is an approximation of the subsurface and often not a representation of the true geology.

Interpreted seismic reflections are based on the acoustic seismic response which resembles differences in impedance between different earth materials. Continuous reflections are typically interpreted as horizons representing stratal surfaces, whereas discontinuities are interpreted to represent fault displacements or unconformities. Many efforts have been made to automate fault tracking based on reflection discontinuities. Examples are algorithms such as semblance, a continuity measurement (Marfurt et al., 1998), variance, a discontinuity measurement (Randen et al., 2001) and most recently an extraction method based on fault surface computation and extraction (Hale, 2013). Despite the advancements made in autopicking algorithms, not all discontinuities are caused by faults. Reflection terminations can be caused by stratigraphic features such as unconformities or by imaging artifacts (Herron, 2000). Furthermore, subsurface structures maybe invisible or mis-postioned on imaged sections (Lawton and Isaac, 2001). As a result, seismic interpretation often requires validation tools to properly understand the true subsurface structure.

Kinematic balanced-forward models can provide geologically reasonable solutions to ambiguous seismic images. Specifically, in extensional settings, where normal faults dominate the Earth's crust, inclined simple shear modeling can predict a distinct relationship between a fault shape and its hanging-wall deformation. This relationship has been analyzed by physical modeling (e.g. Cloos, 1968;

McClay and Ellis, 1987) and quantitative studies (e.g. Gibbs, 1983; White, 1986; Rowan and Kligfield, 1989; Groshong, 1989; Nunns, 1991; Xiao and Suppe, 1992). Dula (1991) compared different algorithms of kinematic modeling showing the inclined-shear model to be the most realistic. Xiao and Suppe (1992) further explained the concept of how hanging-wall deformation is controlled by the shape of the fault. Moreover, concepts of the rollover define how hanging-wall strata deform along active axial surfaces by coulomb shear failure.

In this paper, we create kinematic forward models based on the inclined shear deformation and the rollover theory of Xiao and Suppe (1992). Implementation and model development were undertaken using recently released structural modelling software STRUCTURESOLVER made available to this project. All the created models are balanced (i.e. cross sectional area is preserved). The kinematic models describe how the geometry of a normal fault is related to its hanging-wall strain. We address controlling variables affecting hanging-wall deformation, including the fault shape, amount of sedimentation, slip ratio and shear angles. We then create kinematic forward models to estimate the trajectory of a major normal fault at depth in poorly imaged seismic sections.

Theory and/or Method

In a single normal fault segment, the hanging-wall block subsides with a displacement vector parallel to the fault surface. In the case of a non-planar fault consisting of two segments or more, the hanging-wall block is moved by different displacement vectors during slip. If the hanging-wall block was purely rigid, a void would be created due to movement along the lower fault segment below the fault bend (Fig 1b). However, in reality, overlaying sediments would collapse along a shear axial surface and instantaneously fill the void (Figure 1d). Xiao and Suppe (1992) explained this collapse by Coulomb shear along active axial shear surfaces. The active axial surfaces form at fault bends and are fixed at depth to the footwall cutoffs of those bends.

To illustrate the deformation mechanism along axial shear surfaces, we model a normal fault with a single concave-upward fault bend (Figure 2). In this case, an associated active shear axis forms at the fault bend at which hanging-wall beds collapse antithetically. The position of the active antithetic axis remains fixed at the footwall cutoff of the fault-bend (e.g. blue horizon footwall cutoff in Figure 2). As hanging-wall beds in the upper fault segment move over the fault bend, they deform as a result of passing through the active antithetic shear axial surface. Deformed beds fold around the active shear axis and dip toward the fault surface.

In the case of a convex-upward fault bend (Figure 3), an associated active shear axis forms at the fault-bend, at which hanging-wall beds collapse synthetically. Figure 3 shows a synthetic active shear axis modeled in a single-bend fault. Hanging-wall beds in the lower fault segment (i.e. below the bend before faulting) remain undeformed since they do not pass through the active shear axis. When layers move over a convex-upward fault-bend (Figure 3), the position of the active synthetic axis remains fixed at the footwall cutoff of the fault bend (e.g. the blue horizon footwall cutoff in Figure 3), and beds passing over that fault bend collapse synthetically along the active shear axis causing the beds to dip away from the fault.

The boundary between the deformed and underformed beds in the lower fault segment defines the position of an inactive shear axis. This inactive axis remains parallel to the active axis in all stages of

deformation. In an undeformed state, active and inactive axes are aligned in the same position at the fault bend (Figures 2a and 3a). The inactive shear axis terminates in the hanging-wall cutoff at the fault bend prior to slip and moves with the hanging-wall block along the fault surface during slip (e.g. blue horizon hanging-wall cutoff at fault bend in Figures 2 and 3).

The active and inactive shear axes form together a kink band which defines a deformation zone. The width of this deformation zone is proportional to the fault slip. As slip increases, the deformation zone widens. All deformed beds, which passed through the active axial surface, are contained within this zone. As hanging-wall layers slip along the fault surface, new accommodation space is created above subsiding hanging-wall allowing new sediments to be deposited.

Deposition during faulting creates growth strata (Figure 4). The model shows growth beds (white horizons in Figure 4) are thickest above the steepest fault segment. Similar to pre-growth beds, growth deposits start to collapse and rollover as they pass through the active shear axis, which remains stationary throughout all stages of deformation. In contrast, growth sediments that did not pass through the active shear axis remain undeformed (i.e. deposited to the right of the active shear axis or in the footwall). The position of the inactive axial surface varies within the growth section depending on the expansion ratio, which is directly determined by sedimentation and slip rates (Xiao and Suppe, 1992; Spang and Dorobek, 1998). As a result, the dip of the surface connecting the active and inactive axial surfaces varies as expansion rates of beds change. This connecting surface is called growth axial surface (purple dashed line in Figure 4) and is created when the syntectonic sedimentation rate exceeds the slip rate; i.e. accommodation space above pre-growth beds is overfilled (Spang and Dorobek, 1998). The growth axial surface along with the fault and the two shear axial surfaces define a deformation zone within which all deformed beds are contained. Growth axial surfaces can possibly be interpreted on seismic sections at the upward terminations of secondary antithetic and synthetic faults in the hanging wall (e.g. Shaw et al., 1997; Spang and Dorobek, 1998). For a given fault shape, the dip of growth axial surface is directly proportional to the amount of sedimentation and inversely proportional to the slip and expansion rate. More specifically, the growth axial surface can develop a curvature that is concave-up with increasing overfill sedimentation rate and convex-up with decreasing overfill sedimentation rate. The growth axial surface in Figure 4 (purple dashed-line) is straight because it was modeled at a constant slip-to-sedimentation rate. More on growth axial surfaces is discussed by Xiao and Suppe (1992), Shaw et al. (1997), and Spang and Dorobek (1998).

Another factor affecting the deformation is the shear angles at which beds collapse. The shear angle is the acute angle between the vertical and the inclined shear axis (White et al., 1986). Figures 5 and 6 show the sensitivity of the deformed beds geometries to shear angles at concave- and convex-upward fault bends. For an antithetic shear axis, the model shows the dip of deformed hanging-wall beds decreases as the shear angle increases. In contrast, the dip of deformed hanging-wall beds increases as the shear angle increases for a synthetic shear axis.

Examples

The concepts discussed in the previous section are very practical for assisting in seismic interpretation. We show an example by modeling a seismic section from a 3D survey in the Taranaki Basin, New Zealand. Our structural interpretation of this survey showed north-east trending normal

faults dominating the shallow reflections (Figure 7). Tracing alignments of amplitude terminations on time slices indicates the geometry of fault surfaces in the strike direction. Computed attributes based on semblance and variance algorithms were helpful in delineating the shallow fault surfaces, but not the deeper poorly imaged sections. The computed attribute volumes indicated an evidence of possible up-sequence gas flow along some major faults which appear to be cutting through the main proven reservoir (Alarfaj and Lawton, 2012). Similar indications of gas migration along normal faults were characterized in studies within the Taranaki Basin (e.g. Ilg et al, 2012). We use kinematic forward models related to the concepts of extensional fault-bend folding to solve for ambiguities in our seismic interpretation. In this case, the geologic models served as a valuable tool for understanding the structural evolution in the basin as well as evaluating the sealing and trapping integrity interpreted from the seismic volume.

We show a model of a time migrated seismic section almost parallel to the dominant dip direction (Figure 8). We are interested specifically in the major fault in the middle of the section which exhibits listric characteristic with its thickening hanging-wall blocks tilting toward the fault surface. The listric-like shape implies that the fault's dip continues to decrease gradually until it flattens out at depth. However, the exact fault shape is difficult to trace at deep reflections in the section. We model this master fault based on knowledge of its shape at the shallow reflections and the horizons cutoffs at the fault surface. The interpreted horizons (light green and light blue in Figure 8) indicate the observed geometry of beds from the seismic section. Secondary antithetic and synthetic faults indicate the orientation of the active shear axial surfaces and the shear angles. The master fault shape is therefore modeled by series of fault bends; concave-upward bends at deep terminations of antithetic faults and convex-upward bends at deep terminations of synthetic faults with the master fault. Adjusting the shape of the modeled fault changes the geometry of the modeled hanging-wall beds. The modeled hanging-wall beds (dark green and dark blue in Figure 8) are matched with the observed seismic horizons to validate the model and confirm the fault's shape.

We also modeled different scenarios for the fault geometry to verify our seismic interpretation. One of the modeled scenarios is a listric shape that flattens out at shallower reflections. We examined each scenario by varying the fault shape at depth while matching the modeled hanging-wall geometry with the ones observed in the seismic sections. A mismatch between the modeled and observed horizons indicates an incorrect fault geometry.

RESULTS AND DISCUSSION

The modeled fault geometry adequately resembles the observed shallow structure. The models suggest that the deformations in the hanging-wall structure were mainly controlled by movement along the underlying major fault surface. The bends in this major fault were constructed to match the interpreted major fault trace and were inferred by secondary faults where the major fault trace is not visible. The dips of secondary faults observed on the seismic sections are generally 63-68 degrees indicating shear angles of about 22-27 degrees measured from the normal to horizontal beds. Some of the deformed hanging-wall beds have passed through antithetic and synthetic shear axial surfaces resulting in an apparent underformed horizontal orientation. The model shows a ramp-and-flat geometry of the major fault which offsets the basement at depth of about 6 km (about 3.3 seconds TWT).

We modeled different shapes for the major fault at depth to validate our interpretation. One of the examined scenarios is for a fault shape that flattens out above the basement (Figure 9). The model shows a mismatch between the modeled shallow horizons and interpreted horizons in the seismic section. We therefore conclude this geometry to be invalid for the interpreted master fault.

The structural orientations of the major fault and hanging-wall blocks appear to be consistent throughout the 3D seismic survey. We modeled consecutive normal-to-strike lines to map the surface of the master fault (Figure 10).

Deformation in the subsurface is affected by different variables, including the fault shape and its total slip, sedimentation rate relative to the slip, and the direction of hanging-wall collapse along shear axes, and compaction. Our models consider all these variables except for compaction. Although compaction can alter the fault shape and its associated hanging-wall deformation, Xiao and Suppe (1992) concluded that except for uncommon conditions, the effect of compaction can be neglected when modeling in the compacted state (i.e. seismic sections).

Conclusions

The unique relationship between fault shape and hanging-wall deformation during extension can be described by kinematic forward models using inclined-shear method. We modeled rollover geometry with different fault bends, sedimentation and slip ratios, and shear angles. An example of kinematic forward models were constructed to predict a fault deep shape in the interpretation of a 3D seismic survey in the Taranaki Basin, New Zealand, from seismic images where the fault is not easily interpretable at depth. The model suggests that the overall structure is controlled by the geometry of the major normal fault which cuts through the basement

Acknowledgements

We thank Saudi Aramco and CREWES sponsors for supporting this research. We also thank Nunns and Rogan LLC for providing the modeling software STRUCTURESOLVER. We especially appreciate Dr. Alan Nunn for his consultation in using the software. Seismic data were obtained from the NZ government. Saudi Aramco is thanked for financial support of the first author.

References

Alarfaj, M., and Lawton, D. C., 2012, Interpreting fault-related gas leakage, CREWES Research Report, 25, 1-10.

Cloos, E., 1968, Experimental analysis of Gulf Coast fracture patterns: AAPG Bulletin, v. 52, 420-444.

Dula Jr, W. F., 1991, Geometric Models of Listric Normal Faults and Rollover Folds (1); AAPG Bulletin, 75(10), 1609-1625.

Gibbs, A. D., 1983, Balanced cross-section construction from seismic sections in areas of extensional tectonics: Journal of Structural Geology, v. 5, p. 1-39.

GROSHONG, R. H., 1989, Half-graben structures: Balanced models of extensional fault-bend folds; Geological Society of America Bulletin, 101(1), 96-105.

Hale, D., 2013, Methods to compute fault images, extract fault surfaces, and estimate fault throws from 3D seismic images: Geophysics, v. 78, No. 2, O33-O43.

Herron, D. A., 2000, Pitfalls in seismic interpretation: Depth migration artifacts: The Leading Edge, v. 19, No. 9, 1016-1017.

Ilg, B. R. , Hemmings-Sykes, S., Nicol, A., Baur, J., Fohrmann, M., Funnell, R., and Milner, M., 2012, Normal faults and gas migration in an active plate boundary, southern Taranaki Basin, offshore, New Zealand: AAPG Bulletin, v. 96, No. 9, 1733-1756

Lawton, D. C., Isaac, J. H., Vestrum, R. W., & Leslie, J. M., 2001, Slip-slidin'away—some practical implications of seismic velocity anisotropy on depth imaging: The Leading Edge, 20(1), 70-73.

Marfurt, K., R. Kirlin, S. Farmer, and M. Bahorich, 1998, 3-D seismic attributes using a semblance-based coherency algorithm: Geophysics, 63, 1150–1165

McClay, K. R., & Ellis, P. G., 1987, Geometries of extensional fault systems developed in model experiments; Geology, 15(4), 341-344.

Nunns, A. G., 1991, Structural Restoration of Seismic and Geologic Sections in Extensional Regimes (1); AAPG Bulletin, 75(2), 278-297.

Randen, T., S. Pedersen, and L. Sonneland, 2001, Automatic extraction of fault surfaces from three-dimensional seismic data: 71st Annual International Meeting, SEG, Expanded Abstracts, 551–554.

Rowan, M. G., & Kligfield, R., 1989, Cross section restoration and balancing as aid to seismic interpretation in extensional terranes; AAPG bulletin, 73(8), 955-966.

Shaw, J. H., Hook, S. C., & Sitohang, E. P., 1997, Extensional fault-bend folding and synrift deposition: An example from the Central Sumatra Basin; Indonesia. AAPG bulletin, 81, 367-379.

Spang, J. H., & Dorobek, S. L., 1998, Using Antithetic Normal Faults to Map Growth Axial Surfaces.

White, N. J., J. A. Jackson, and D. P. Mckenzie, 1986, The relationship between the geometry of normal faults and theat of the sedmentary layers in their hanging walls: Journal of S

Xiao, H., & Suppe, J., 1992, Origin of Rollover (1); AAPG Bulletin, 76(4), 509-529.

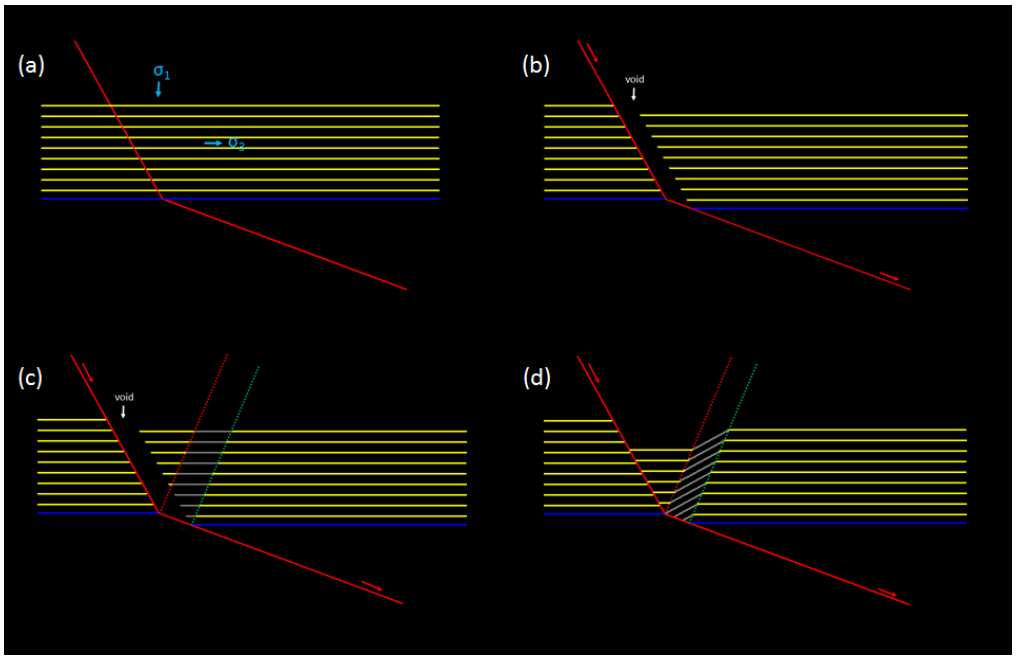

FIG. 1. Inclined simple shear along the active axial surface by movement over a concave-upward fault bend. Hanging-wall strata collapse instantaneously to fill a void created by extension.

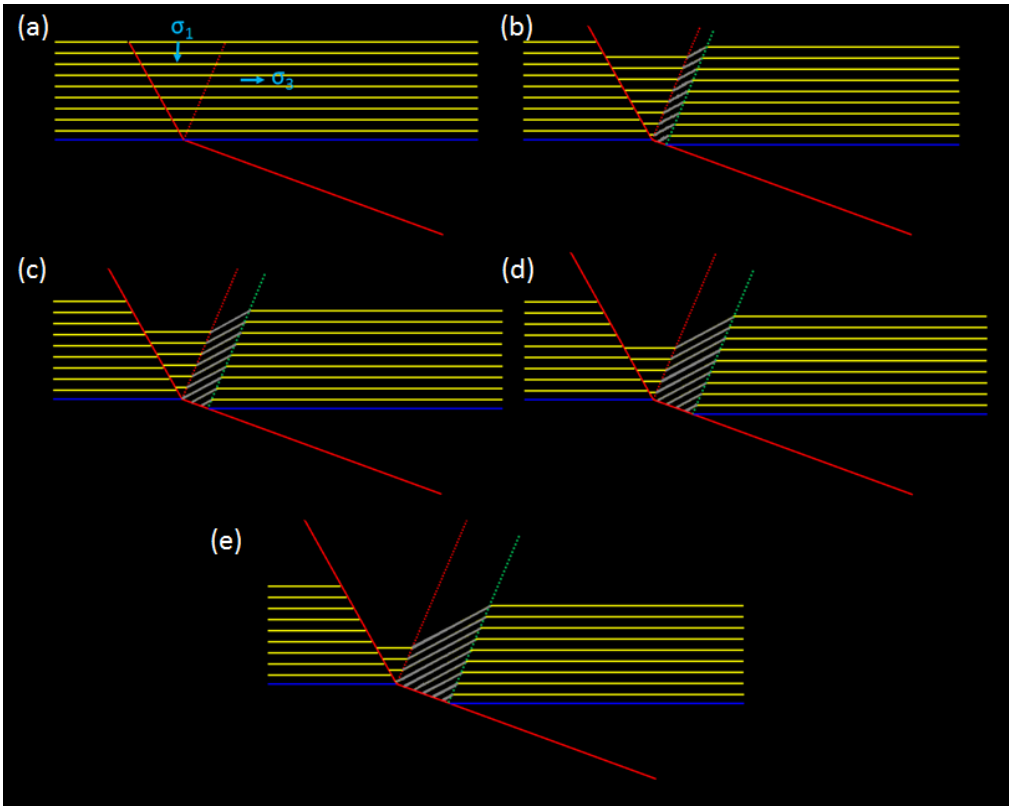

FIG. 2. Sequential stages of deformation over a concave-upward fault bend. Grey lines indicate deformed hanging-wall beds within a kink band.

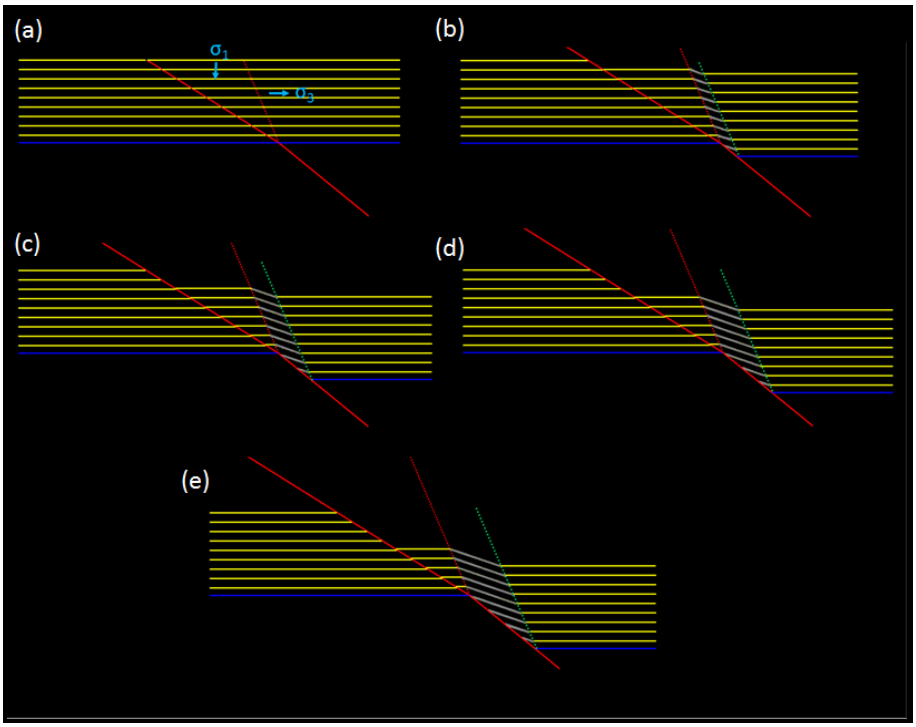

FIG. 3. Sequential stages of deformation over a convex-upward fault bend. Grey lines indicate deformed hanging-wall beds within a kink band.

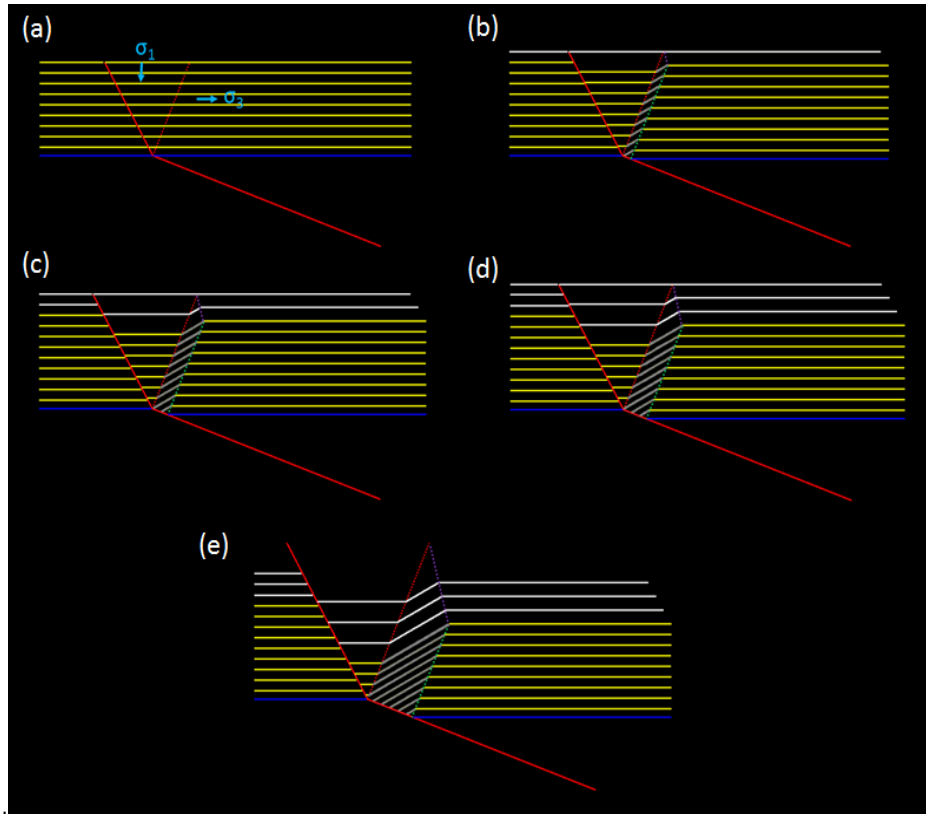

FIG. 4. Sequential stages of deformation for syntectonic deposition over a concave bend. White horizons indicate growth sediments. Grey lines indicate deformed hanging-wall beds within a kink band.

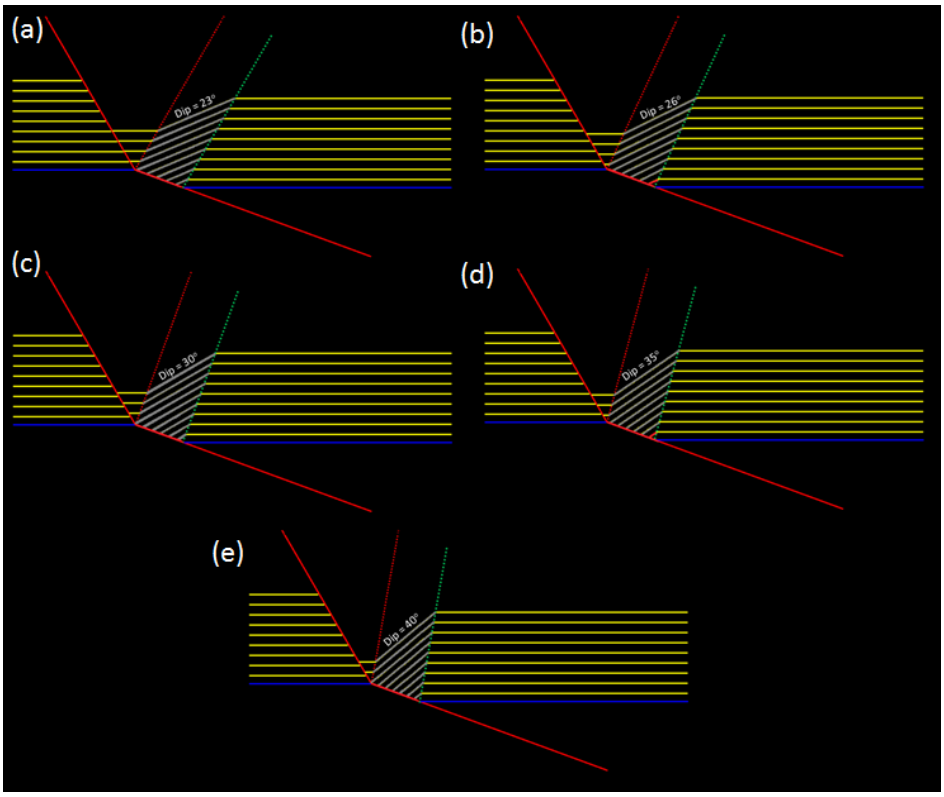

FIG. 5. Sensitivity to changes in antithetic shear angles: a) 30^{o} b) 25^{o} c) 20^{o} d) 15^{o} e) 10^{o}

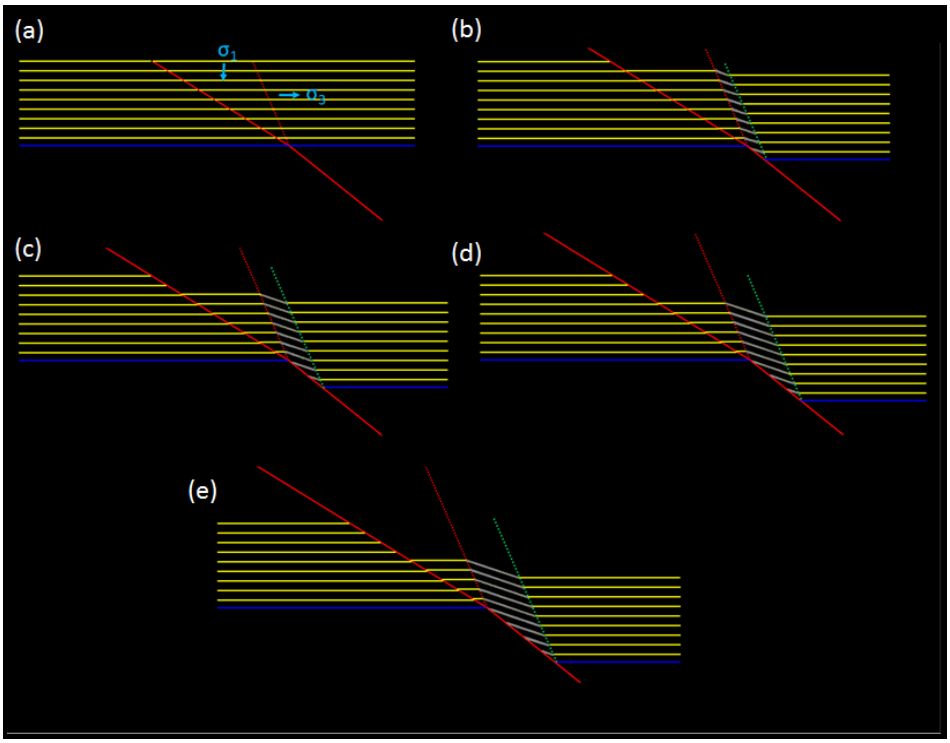

FIG. 6. Sensitivity to changes in synthetic shear angles: a) -30^{o} b) -25^{o} c) -20^{o} d) -15^{o} e) -10^{o}. Dip of layers in grey decreases as the synthetic shear angle decreases.

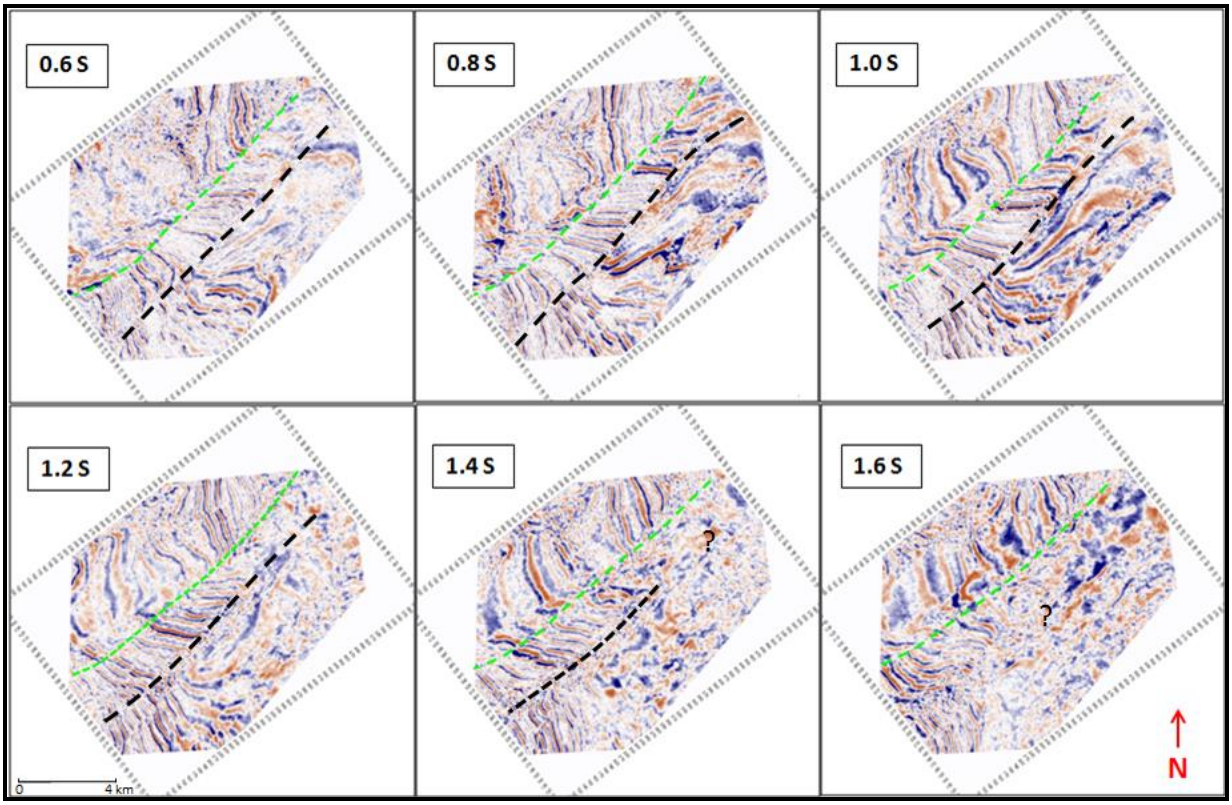

FIG. 7. Time slices showing an approximate location of the master fault in black dashed-line and an associated antithetic fault in green dashed-line. Tracing the alignments of event terminations indicates the strike of faults. The master fault is more difficult to trace with increasing depth.

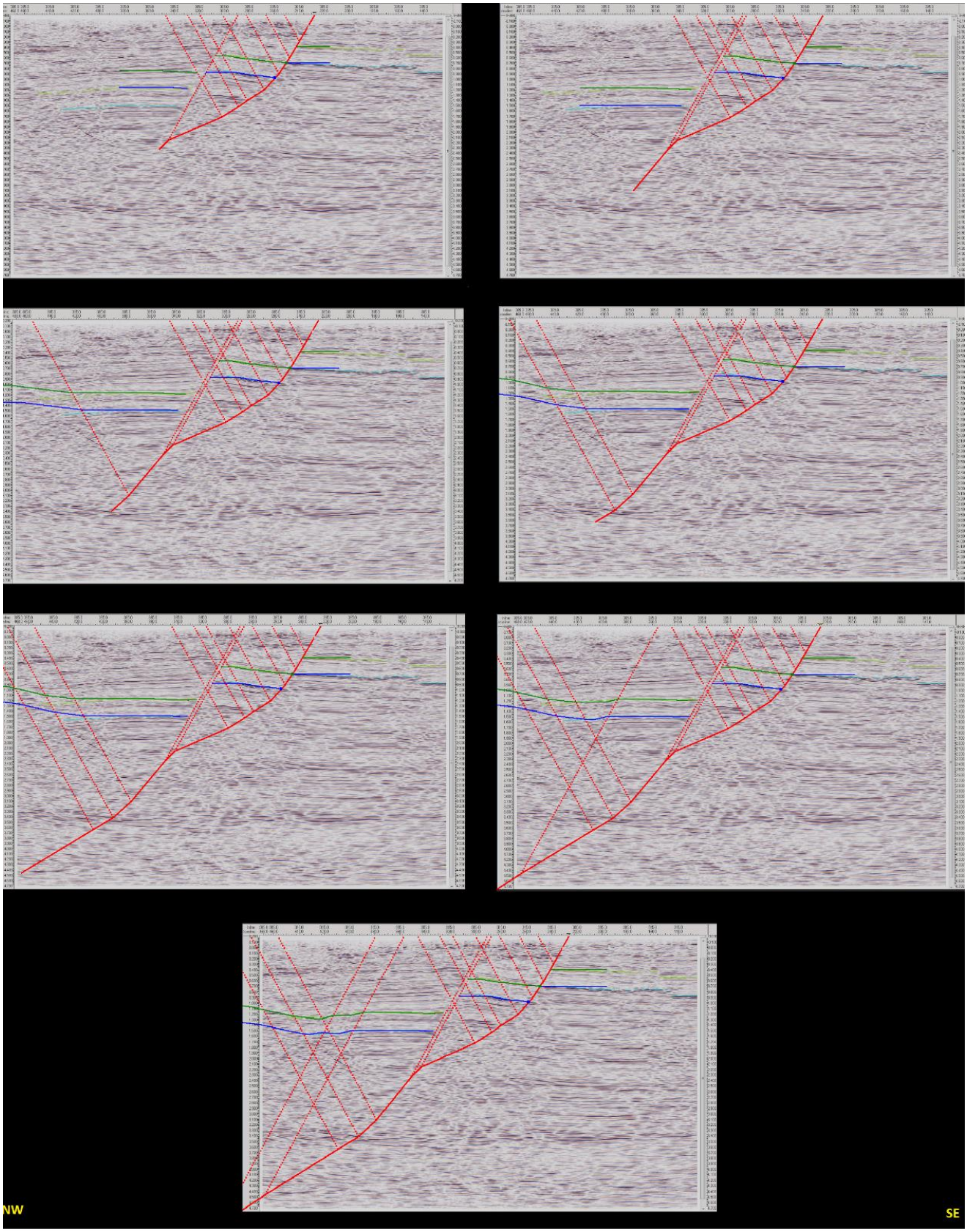

FIG. 8. Kinematic forward modeling for fault prediction. Light green and blue are interpreted seismic horizons. Dark green and blue are modeled horizons Grey horizons indicates observed layers from the seismic section

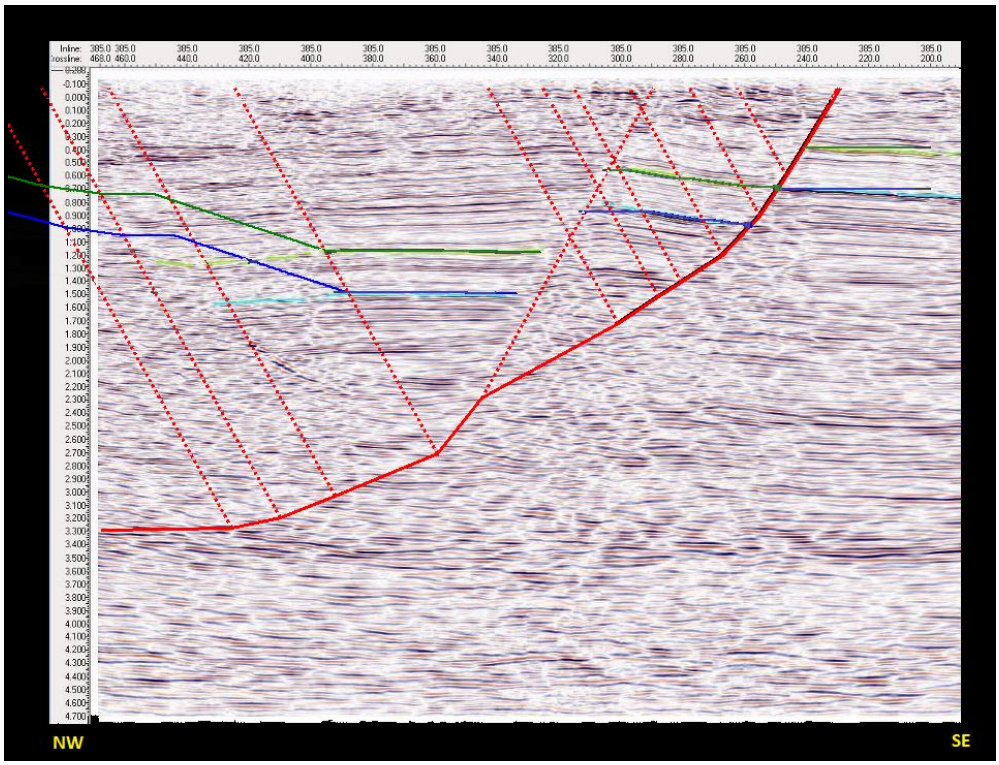

FIG. 9. Incorrect model showing deformation caused by a listric fault. Grey horizons indicates observed layers from the seismic section

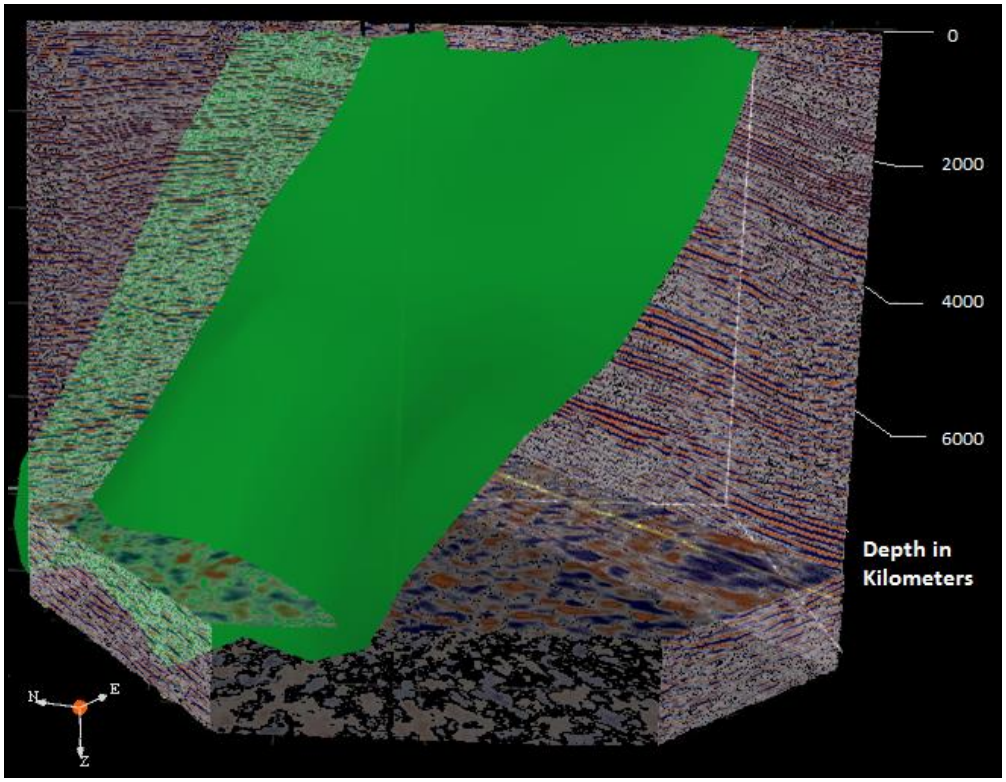

FIG 10. The fault surface interpreted from a sequence of inline models on a depth-converted volume.